Potential use of resonance frequencies in microseismic interpretation

J. B. TARY and M. VAN DER BAAN, University of Alberta

Continuous passive recordings of microseismic experiments can be used to detect and trace the modifications in frequency content during hydraulic fracturing or heavy-oil steam injection. We analyze the performance of four different time-frequency representations, namely the short-time Fourier transform, the S-transform, the continuous wavelet transform, and the autoregressive method, on a real microseismic data set of intermediate quality. We show that time-frequency transforms provide an efficient tool to highlight time-varying resonance frequencies occurring during reservoir fracturing. Four distinct resonance frequencies at ~17, ~35, ~51, and 60 Hz are observed during two experiments using the same experimental setup.

The causes of resonance frequencies in hydrofracture experiments are then carefully reviewed to identify the potential causes of the observed values and illustrate how their analysis may help in reservoir management. In our case, resonance frequencies at the receiver side are anticipated to be outside the observed frequency band. In our borehole acquisition configuration, where the geophones and the stimulated reservoir

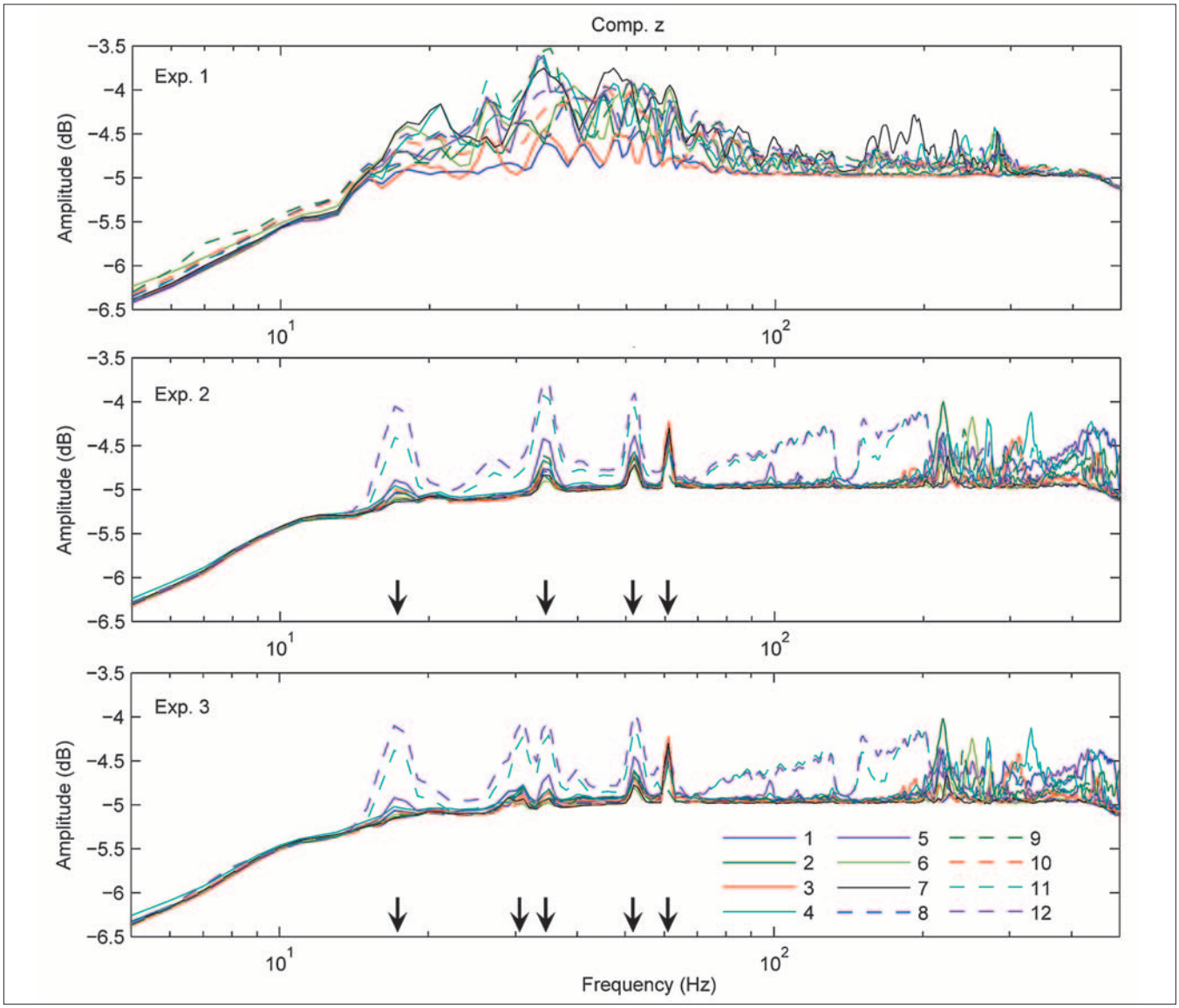

Figure 1. *Mean Fourier amplitude spectra for the 12 geophones (vertical component) of the three experiments (geophone 12 being the deepest one). These spectra are obtained by first computing the STFT (window = 1 s), and then averaging over the complete signal to obtain an averaged spectra for the complete experiment. The data are low-pass filtered at 500 Hz as no significant energy is in the frequency band 500-2000 Hz. Note that for the second and third experiments, resonance frequencies are clearly visible at ~17, ~31 (second experiment only), ~35, ~51, and ~60 Hz for most stations (black arrows).*

interval are approximately at the same depth, wave propagation is predominantly horizontal and resonance frequencies caused by path effects will be limited. Therefore, the observed resonance frequencies likely result from source effects including resonance of fluid-filled cracks or successions of small repetitive events. The length of a fluid-filled crack corresponding to a resonance frequency of ~17 Hz is in the order of a few tens of meters. We postulate that this corresponds to the length of interconnected fractures and thus represents mesoscale deformations occurring inside the reservoir caused by hydraulic fracturing, lying between micro-earthquakes with slip surfaces of a few tens of centimeters to a few meters and the total stimulated reservoir volume.

Introduction

To extract tight hydrocarbons or enhance hydrocarbon recovery in general, operators appeal more and more often to hydraulic fracturing, where fluids are injected into the reservoir at high pressure to create new fracture networks, thus increasing permeability and hydrocarbon drainage. Fracturing experiments are often monitored using microseismic recordings, where geophones are used to record and locate the numerous micro-earthquakes generated during fracturing. In the case of tight hydrocarbons, it is often assumed that the stimulated reservoir volume is proportional to the extent of the microseismic event cloud. Microseismic monitoring currently relies predominantly on mapping brittle failure as expressed by

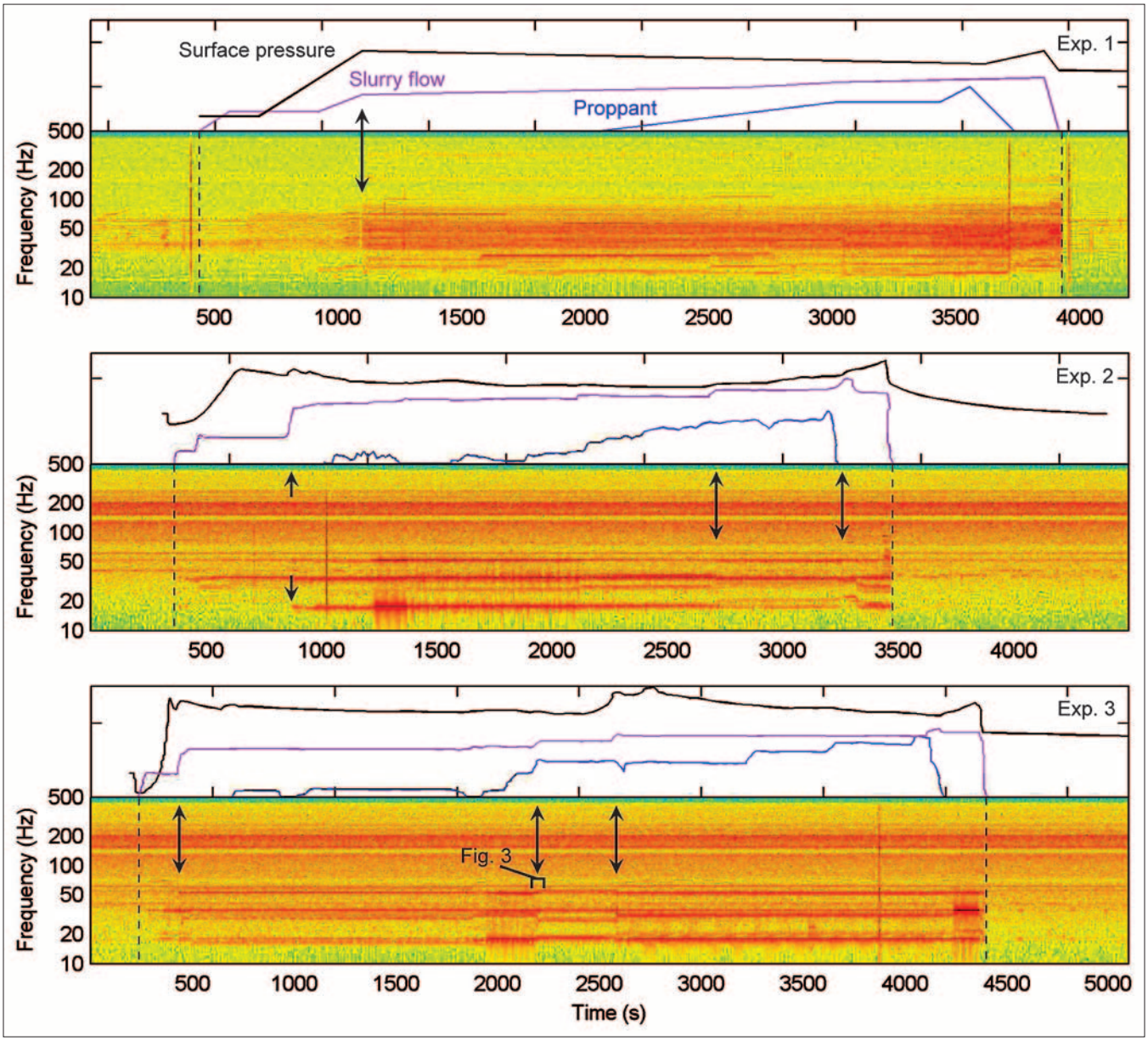

Figure 2. *Treatment curves and STFT of the three experiments (deepest geophones, vertical component). The data are downsampled from 4000 Hz to 1000 Hz prior to the computation of the time-frequency transforms in order to decrease the computation time. Hot colors correspond to high amplitudes. A window of 4 s with 50% overlap is used to compute the STFT. On the treatment plots, the black line corresponds to surface pressure, the pink line corresponds to slurry flow and the blue line corresponds to proppant concentration. Black arrows indicate some simultaneous variations of the slurry flow and the signal frequency content. The segment of data used for Figure 3 is also indicated. Note the strong change in frequency content between the first experiment and the two following ones.*

a microseismic event to delineate the deformation occurring inside the reservoir.

This assumption might not be correct as orders of magnitude of the total energy injected into the system are not accounted for compared with the energy released by the recorded microseismicity (Maxwell, 2009). In addition to fluid leak-off and fluid friction inside the formation and well, brittle failure is unlikely to be the only kind of deformation releasing energy during hydraulic fracturing. Significant amounts of energy are anticipated to be associated with other kinds of deformations such as tensile fracturing or slow deformation (Chorney et al., 2012 in this special section). Such rock deformations are unlikely to be detected by focusing on triggered events only, because this implies sharp signal onsets (Bame and Fehler, 1986).

On the other hand, continuous recordings and their time-frequency analysis also provide valuable information as illustrated by Das and Zoback (2011) and Pettitt et al. (2009). Das and Zoback (2011) use the short-time Fourier transform (STFT) to design a band-pass filter in order to remove background noise and undesired signals. This simple procedure enables them to detect signals with particular frequency contents such as long-period and long-duration microseismic events (LPLD).

Pettitt et al. use the STFT to find possible correlations between variations in the frequency content of the microseismic recordings, the treatment conditions and the occurrence of microseismic events. They observe a direct correspondence between variations in the slurry injection rate and the combined energy emitted by concurring events. More surprisingly, their time-frequency spectrum shows stable spectral lines (that is, resonance frequencies) persistent throughout the five hours of recording, even in between fracturing stages, displaying only variations in amplitude. In one particular stage, microseismic events occur simultaneously in two separate lithologies at different depths whereas injection occurs only into the lower unit. No seismicity is detected revealing potential leak-off or fluid diffusion through the intermediate layer. The time-frequency spectrum shows, however, a gradual decrease in amplitude of several resonance frequencies, potentially indicating the coalescence of micro-fractures enabling fluid migration without producing brittle failure.

Both studies demonstrate that time-frequency analysis of continuous recordings can provide valuable information on the actual reservoir behavior, complementary to conclusions derived from the analysis of triggered events. Time-frequency analyses are particularly suited to study long-duration, nonstationary phenomena that may take place inside the reservoir.

A first crucial step is to ensure accurate determination of the frequency content of the continuous recordings. Many different time-frequency transforms exist, each with their own advantages and inconveniences. In the next section, we briefly describe the well-known STFT, then two transforms with variable time-frequency resolution, namely the S-transform (ST; Stockwell et al., 1996) and the continuous wavelet transform (CWT; Daubechies, 1992), and finally present an adaptation of the autoregressive method (AR; Burg, 1972; Claerbout, 1985). Each transform is applied to a real data set of intermediate

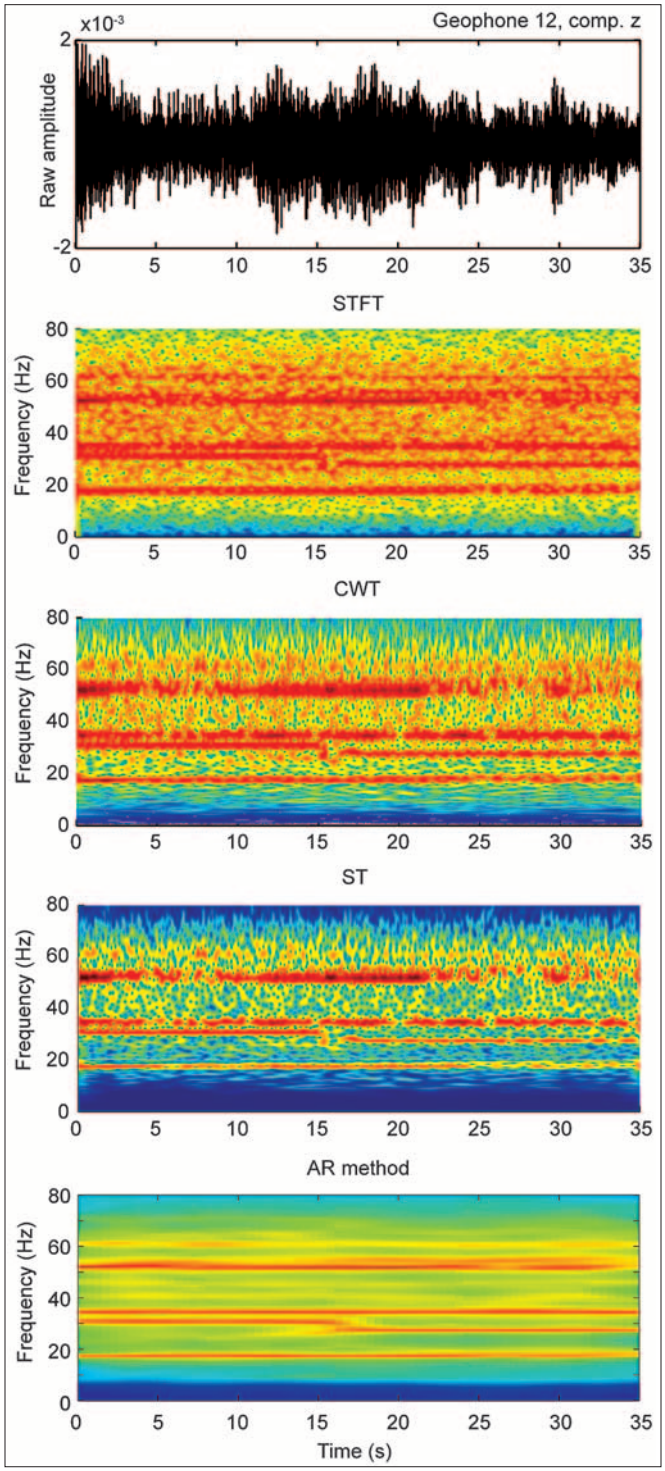

Figure 3. *The four time-frequency transforms applied to a sample of data of the third experiment corresponding to the segment between 2175 and 2210 s in Figure 2 (vertical component of the deepest geophone). The data are downsampled from 4000 Hz to 160 Hz prior to the computation of the time-frequency transforms. Hot colors correspond to high amplitudes. A window of 1 is used to compute the STFT. The CWT uses a Morlet wavelet with a high number of cycles (~32). The AR method uses a window length of 20 s (overlap of 95%) and 30 coefficients. The same resonance frequencies shown in Figure 1 can be found on the STFT, CWT, ST, and AR method plots.*

quality to compare their decomposition results.

Then, in the following section, we review the possible causes of the resonance frequencies revealed by the time-frequency transforms. Indeed, resonance frequencies can arise from source, path and receiver effects. Finally, we discuss the most likely origins of the resonance frequencies in this data set.

Time-frequency transforms

The four time-frequency transforms described hereafter will be used to detect possible frequency content changes of the ambient noise during fracturing experiments. These representations are specially adapted to analyze the frequency content of nonstationary signals (Reine et al., 2009).

The STFT is a simple technique, displaying the Fourier spectra of successive overlapping windows of a signal. The window function used in this study is the Hann function. Very long data sequences can be analyzed by simply increasing the size of the window and decreasing the overlap. Because the window length is fixed independently of the investigated frequency, the STFT has a constant time-frequency resolution. Therefore, signals with frequency bandwidth superior to three orders of magnitude (from 1 to 1000 Hz for example) cannot, for practical purposes, be studied with this transform.

Transforms with variable time-frequency resolutions like the ST and the CWT are essential in these cases. The CWT and ST achieve with variable time-frequency in different ways. For the ST, the signal is first windowed by a Gaussian window, the size of this window being inversely proportional to the frequency investigated (Stockwell et al.). The CWT uses a different basis function, called the mother wavelet (Daubechies). We use the Morlet wavelet as mother wavelet because of its high similarity to seismic wave packets and its smoother character (e.g., compared to the Mexican hat wavelet). A family of wavelets is generated by translating and dilating the mother wavelet. A scale factor is used to stretch and squeeze the mother wavelet in the time domain as a function of the analyzed frequency. In brief, there is an inherent trade-off between frequency and time resolution. At low frequencies, a high frequency resolution but a low time resolution is obtained by increasing the size of the Gaussian window (ST) or by stretching the mother wavelet (CWT), and conversely these transforms yield a high temporal resolution but poor frequency resolution for high frequencies. Another parameter, the number of oscillations in the mother wavelet, can also be used to increase the frequency resolution at the expense of decreasing the time resolution and vice versa. The trend between time and frequency resolutions is often summarized by the expression "constant Q", which means that these transforms have a constant ratio of central frequency to frequency bandwidth (Brown, 1991). The frequency bandwidth is defined as the ratio between sampling frequency and window length.

The AR method is a linear prediction filter that tries to predict future samples using the previous ones, minimizing the errors in a least-squares sense between the recorded signal and a predicted filter (Burg, 1972; Claerbout, 1985). The AR method depends on two parameters specified a priori, namely a fixed number of coefficients for the AR filter (i.e., a fixed number of frequencies) and the length of the window on which the AR filter is "trained." These two parameters have to be optimized independently by training the algorithm on a representative part of the data. Indeed, the outcome of the AR method is significantly improved if optimal values for the two parameters are employed. The parameterization also depends on the objectives (i.e., if one wants a global or a detailed picture). Here, we determined the optimal pair of parameters by minimizing the errors in a least-squares sense between the Fourier spectrum of the windowed signal and the spectrum obtained with the AR method using different pairs of parameters. Once the optimal parameters are determined, they are used to compute the AR method on the complete seismic trace. Likewise for the STFT, the window is then slid along the complete signal to estimate the local frequency content. The frequency resolution is proportional to the number of coefficients of the AR filter and the time resolution is inversely proportional to the length of the overlapping windows.

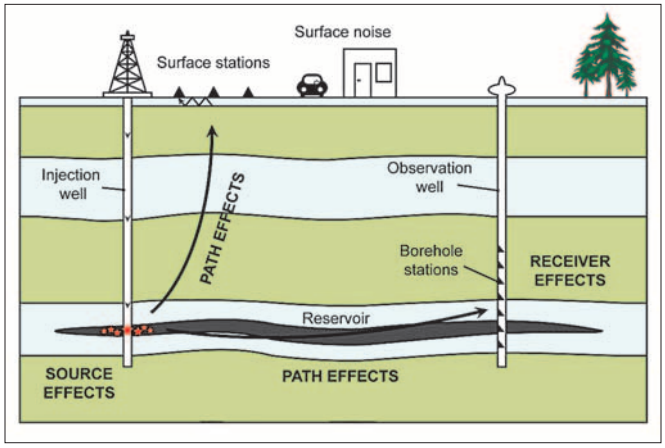

Figure 4. *Sketch of a typical configuration of hydrofracture experiments. Seismic waves generated by fracturing or perforation shots (red stars) travel through the Earth (reservoir or geologic formations), and are eventually recorded by seismic stations either on the surface or in the observation well.*

Observed resonances

When applied to data, these methods give somewhat different representations of the frequency content of the continuous signals. Three fracturing experiments with continuous recordings of ~1–2 hours each were selected to evaluate the capability of each time-frequency transform to detect resonance frequencies. The fracturing experiments were recorded by 12 three-component geophones sampled at 4000 Hz, leading to a usable frequency bandwidth of 10–2000 Hz. The geophones were installed in a deviated borehole during the first experiment. During the two following experiments, different injection and observation wells were used, ~3.4 km away from the first experiment. In the latter two experiments, the string of geophones was deployed in a vertical borehole.

The collected data are of intermediate quality with high amplitude noise. Depending on the station and the experiment, the level of noise as well as its frequency content change significantly (Figures 1 and 2). In all experiments, the amount of recorded signal energy is proportional to the slurry flow as

noticed for instance by Pettitt et al. as well (Figure 2). No clear resonance frequencies are visible though for the first experiment.

For experiments 2 and 3, four resonance frequencies are clearly visible at ~17, ~35, ~51, and 60 Hz (Figure 1). For experiment 3, an additional resonance frequency is visible at ~31 Hz. The 60-Hz one corresponds to the electric current and its amplitude is almost constant for all geophones, contrary to the others which have a complex amplitude pattern. The amplitudes of these resonance frequencies are higher on the deepest geophones, followed by geophones five and four.

The evolution of the frequency content of 35 s of the third experiment, corresponding to the segment between 2175 and 2210 s in Figure 2, is presented in Figure 3 (vertical component of the deepest geophone). Five frequency lines, corresponding to those observed on the averaged Fourier transform (Figure 1), are visible on the time-frequency maps of the four transforms. Resonance frequencies are consistent between the different time-frequency transforms although the images display variations in their details. The background colors in the STFT and the AR method are mostly even, indicating the presence of a uniformly distributed background noise, whereas the CWT and ST techniques bring out the resonance frequencies more sharply. By design though, the AR method approach has possibly best tracked the temporal variations in resonance frequencies.

All four analysis techniques indicate that the frequency and amplitude of these spectral lines change over time. In Figure 3, we observe a change of few Hz of one of the frequency lines (~31 Hz) between 15 and 17 s, while the frequency line at 51 Hz almost disappears around 22 s. These changes are correlated with an increase of the slurry flow (Figure 2).

In the following section we will review the possible causes for these resonance frequencies.

Causes of resonance frequencies

Resonance frequencies can be generated by source, path, or receiver effects (Figure 4). Each effect has to be considered separately to determine the origin of a particular resonance frequency.

Amplitudes and frequency ranges of resonance frequencies because of receiver effects depend on the experimental setup. Seismic stations located on the surface are commonly contaminated by anthropogenic noise (cars, drilling operation, etc.) and environmental noise (diurnal temperature changes for example). The uppermost, unconsolidated ground layer can also act as a low-velocity waveguide and create resonance frequencies. In our case, the seismic stations are deployed in boreholes. Even though these geophones are then away from anthropogenic noises, the design of the borehole itself (i.e., a finite cylinder pushed in the ground) and the presence of the geophones also produce resonance frequencies (Sun and McMehan, 1988; St-Onge and Eaton, 2011). These resonance frequencies are produced by constructive interferences of waves propagating inside the pipe (tube waves) and in the casing (Figure 5). Every discontinuity inside the borehole, such as changes in the borehole geometry and material (from steel to cement

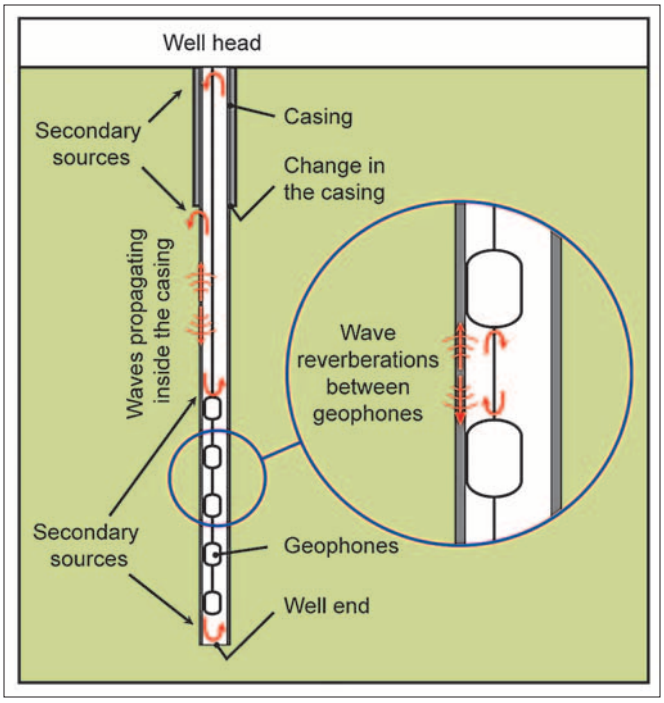

Figure 5. *Sketch illustrating the possible causes of resonance frequencies because of receiver-side effects.*

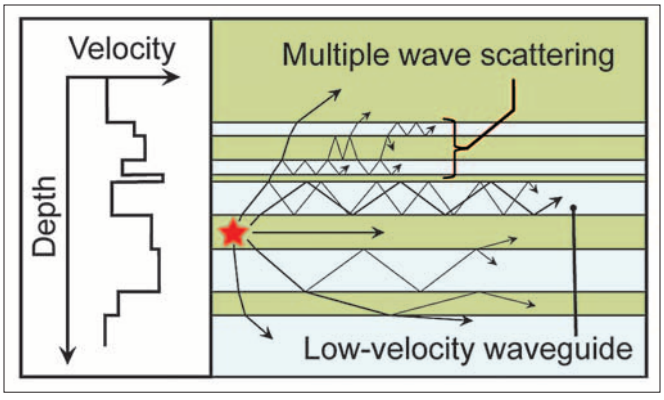

Figure 6. *Sketch illustrating the possible causes of resonance frequencies because of path effects. The seismic waves generated by a source (red star) travel through layers with different velocities. These waves will be reflected and transmitted at layer boundaries, or can be trapped in a low-velocity waveguide.*

casing for example) or the presence of tools inside the pipe, will act as a secondary source and in turn could generate resonance frequencies. The reverberations of the waves between the discontinuities created by an equally spaced set of geophones in the borehole could produce resonances at frequencies proportional to the spacing length and the P-wave velocity of the casing (onto which the geophones are clamped). Or more insidiously, resonance frequencies can also be introduced if geophone clamping or internal damping is defective.

Before reaching the receivers, resonance frequencies can also be produced along the raypath (Figure 6). Constructive and destructive wave interferences in low-velocity waveguides is a well-known mechanism, especially for the study of sedimentary basins and the propagation of acoustic waves in the

SOFAR channel in marine environments. The trapping of waves inside the low-velocity layer amplifies wave amplitudes within a given frequency range, which depends on the geometry and the physical properties of this layer (van der Baan, 2009). Low-velocity hydrocarbon reservoirs can act as waveguides. Their properties could then be studied using resonance frequencies.

An apparent enhancement of a particular frequency band can also arise from scattering of multiple waves. Indeed, given a layered medium with stochastic velocity variations with depth, defined statistically by their distribution and standard deviation, wave localization theory shows that a certain frequency band is preferentially attenuated depending mainly on the characteristic scale length of the velocity variations and their magnitude (van der Baan, 2001; van der Baan et al., 2007). This phenomenon can also act as a natural low-pass filter.

Finally, resonances can occur at the source side, such as inside fluid-filled fractures (Figure 7), extensively studied in volcano seismology (e.g., Ferrazzini and Aki, 1987; Chouet, 2003), which generates tremor-like signals. The oscillation inside the resonator is sustained by a "slow wave", whose name varies among authors (Korneev, 2011). In fluid-filled crack models, the frequency response to the crack excitation depends mainly on the crack extent, the parameters of the pressure transient triggering the oscillations (position, area, and source function), and the crack stiffness (Aki et al., 1977; Chouet, 1986). Korneev (2008) compares different estimations of the velocity and attenuation of this "slow wave" and shows that, for low frequencies, the wavelength of the slow wave is compatible with the dimension of in-situ fractures (~10 m at 10 Hz) and could then sustain fluid-filled fractures resonance. Following an approach similar to Ferrazzini and Aki, Korneev also derives a simple formula to calculate the resonance frequency generated by water- or oil-filled fractures.

Resonance frequencies can also result from successive occurrence of small events, such as micro-fractures, repeating with a characteristic periodicity. These small events, called "high frequency mode of failure" by Pettitt et al. appear on time-frequency maps as lines of constant frequency if perfectly periodic.

Different frequency lines can thus correspond to resonators with different shapes and size, a change in the fluids properties, or to the occurrence of repetitive events at different periodicities. A similar mechanism can be invoked for continuous and step changes in the frequency lines.

Interpretation

We will now discuss the possible origins of the resonance frequencies observed during the second and third experiments. The length of the borehole is approximately 2300 m. The velocity of P-waves in the casing cement, determined from the move-out of P-waves recorded during these experiments, is approximately 3800 m/s. The fundamental resonance frequency of the whole borehole is then around 1.7 Hz. The spacing of geophones during these experiments is 10.4 m. The associated resonance frequency is then approximately 365 Hz (St-Onge and Eaton, 2011). No evident resonance because of the instruments was observed. The resonance frequencies because of receiver-side effects are then significantly higher and lower than the resonance frequencies observed (~17, ~31, ~35 and ~51 Hz). A possible contamination by surface noises cannot be ruled out but the fact that the amplitudes of the resonance frequencies are highest on the deepest geophones makes this hypothesis unlikely.

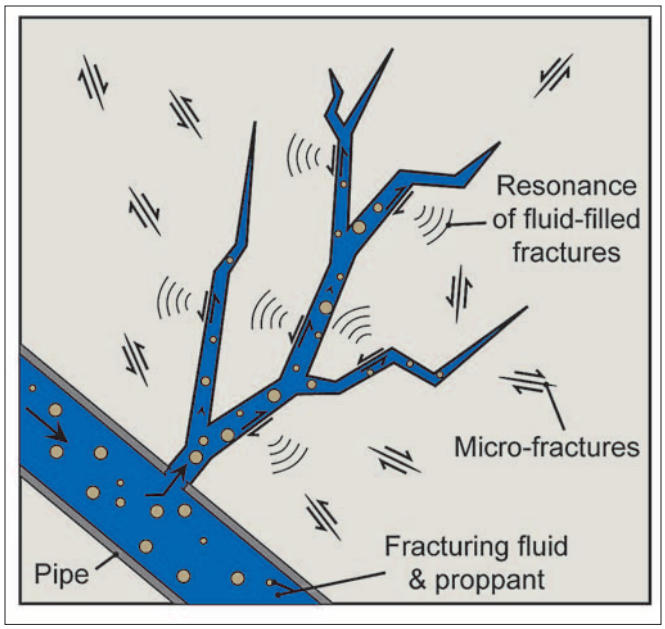

Figure 7. *Sketch illustrating the possible causes of resonance frequencies because of source-side effects.*

The perforation shots, fluid injection, and microseismicity occur all roughly at the same depth as those of the receivers. The waves propagate then predominantly horizontally from the source to the receivers. In this case, scattering of multiple waves and resulting interferences have limited effect on the final signal recorded by the receivers.

We can therefore reasonably assume that both path and receiver effects are less important in our case. The resonance frequencies are then likely mainly related to source effects. They seem to be harmonics of a fundamental frequency of 17 Hz.

Using the simple relationship of Korneev connecting resonance frequencies and fracture dimensions through the medium properties, a resonance frequency of 17 Hz with a fracture thickness of ~0.005 m would correspond to a ~17-m fracture. Crack radii, estimated using Brune's model (Brune, 1970) for micro-earthquakes having magnitude ranging between –3 and –1, are approximately ten times lower (~0.25 < radius < ~2 m). A network of several interconnected fractures would then be necessary to produce the observed resonance frequencies (Figure 7).

Conclusion

At macroscale, the size of the stimulated reservoir volume is determined by the size of the cloud of microseismic events. The distribution and magnitude of the events are used to infer which part, and to what extent, the reservoir permeability was effectively enhanced by the fracturation. At microscale,

we have the individual events, corresponding to brittle failure on slip surfaces. Their source parameters can be estimated using their spectral attributes and crack models. Our working hypothesis is that resonance frequencies can be used to study what lies in between: interconnected parts of the fracture network.

Here, we use time-frequency representations of continuous passive recordings to map the possible variations in frequency content during three hydrofracture experiments. The analysis of continuous recordings using time-frequency transforms shows a clear correlation between the slurry flow and the frequency content of the seismic traces. The four time-frequency representations tested in this study (i.e., STFT, ST, CWT, and the AR method) give consistent results. The differences in frequency content between the first experiment and the two following ones ~3.4 km away, and the differences between our study and the high resonance frequencies reported by Pettitt et al. (>500 Hz), indicate a large variability and that different processes might be dominant in different situations. We are limited in our analysis by the bandwidth of the geophones typically used for hydrofracture experiments. Long-period geophones would be required to look at resonance frequencies used in volcano seismology to study tremors and low-frequency earthquakes (0.01–10 Hz). These could be associated with aseismic, slow-slip events.

The review of the multiple causes of resonance frequencies in fracturing experiments is crucial to further interpret these phenomena, in terms of receiver-side (borehole integrity for example), path (medium properties), or source-side effects (reservoir deformations). More experiments have to be analyzed to validate and understand the underlying phenomena causing the wide range of resonance frequencies in hydrofracture experiments. Nonetheless, this paper shows that time-frequency analysis of continuous microseismic recordings offers significant potential for improved understanding of both brittle failure and aseismic (slow-slip) deformation inside a stimulated reservoir volume. TLE

References

Aki, K., M. Fehler, and S. Das, 1977, Source mechanism of volcanic tremors: fluid-driven crack model and their application to the 1963 Kilauea eruption: Journal of Volcanology and Geothermal Research, **2**, no. 3, 259–287, http://dx.doi.org/10.1016/0377-0273(77)90003-8.

Bame, D, and M. Fehler, 1986, Observations of long period earthquakes accompanying hydraulic fracturing: Geophysical Research Letters, **13**, no. 1, 149–152, http://dx.doi.org/10.1029/GL013i002p00149.

Brown, J. C., 1991, Calculation of a constant Q spectral transform: The Journal of the Acoustical Society of America, 89, no. 1, 425–434, http://dx.doi.org/10.1121/1.400476.

Brune, J., 1970, Tectonic stress and the spectra of seismic shear waves from earthquakes: Journal of Geophysical Research, **75**, no. 26, 4997–5009, http://dx.doi.org/10.1029/JB075i026p04997.

Burg, J. P., 1972, The relationship between maximum entropy spectra and maximum likelihood spectra: Geophysics, **37**, 375–376, doi: http://dx.doi.org/ 10.1190/1.1440265.

Chouet, 1986, Dynamics of a fluid-driven crack in three dimensions by the finite-difference method: Journal of Geophysical Research, **91**, no. B14, 13967-13992.

Chouet, B., 2003, Volcano seismology: Pure and Applied Geophysics, 160, no. 3, 739–788, http://dx.doi.org/10.1007/PL00012556.

Claerbout, J. F., 1985, Fundamentals of geophysical data processing, with applications to petroleum prospecting: Blackwell.

Das, I., and M. D. Zoback, 2011, Long-period, long-duration seismic events during hydraulic fracture stimulation of a shale gas reservoir: The Leading Edge, **30**, no. 7, 778–786, http://dx.doi.org/10.1190/1.3609093.

Daubechies, I., 1992, Ten lectures on wavelets: Society for Industrial and Applied Mathematics (presented at the CBMS-NSF regional conference series in applied mathematics).

Ferrazzini, V. and K. Aki, 1987, Slow waves trapped in a fluid-filled infinite crack: implication for volcanic tremor: Journal of Geophysical Research, **92**, no. B9, 9215–9223, http://dx.doi.org/10.1029/JB092iB09p09215.

Korneev, V., 2008, Slow waves in fractures filled with viscous fluid: Geophysics, **73**, no. 1, N1–N7, http://dx.doi.org/10.1190/1.2802174.

Korneev, V., 2011, Krauklis wave in a stack of alternating fluid-elastic layers: Geophysics, **76**, no. 6, N47–N53, http://dx.doi.org/ 10.1190/geo2011-0086.1.

Maxwell, S. C., J. Shemeta, E. Campbell, and D. Quirk, 2009, Microseismic deformation rate monitoring: EAGE Paper A18, http://dx.doi.org/10.2118/116596-MS.

Pettitt, W., J. Reyes-montes, B. Hemmings, E. Hughes, and R. P. Young, 2009, Using continuous microseismic records for hydrofracture diagnostics and mechanics: 79th Annual International Meeting, SEG, Expanded Abstracts, 1542–1546, http://dx.doi.org/10.1190/1.3255143.

Reine, C., M. van der Baan, and R. Clark, 2009, The robustness of seismic attenuation measurements using fixed- and variable-window time-frequency transforms: Geophysics, **74**, no. 2, WA123–WA135.

St-Onge, A. and D. Eaton, 2011, Noise examples from two microseismic datasets: CSEG Recorder, 36, 46–49.

Stockwell, R. G., L. Mansinha, and R. P. Lowe, 1996, Localization of the complex spectrum: The S transform: IEEE Transactions on Signal Processing, **44**, no. 4, 998–1001, http://dx.doi.org/10.1109/78.492555.

Sun, R. and G. McMehan, 1988, Finite-difference modeling of borehole resonances: Energy Resources, **10**, no. 1, 55–75, http://dx.doi.org/10.1080/00908318808908916.

van der Baan, M., 2001, Acoustic wave propagation in one-dimensional random media: the wave localization approach: Geophysical Journal International, **145**, no. 3, 631–646, http://dx.doi.org/10.1046/j.1365-246x.2001.01405.x.

van der Baan, M., 2009, The origin of SH-wave resonance frequencies in sedimentary layers: Geophysical Journal International, **178**, no. 3, 1587–1596, http://dx.doi.org/10.1111/j.1365-246X.2009.04245.x.

van der Baan, M., J. Wookey, and D. Smit, 2007, Stratigraphic filtering and source penetration depth: Geophysical Prospecting, **55**, no. 5, 679–684, http://dx.doi.org/10.1111/j.1365-2478.2007.00647.x.

Acknowledgments: The authors thank the sponsors of the Microseismic Industry consortium for financial support, and Husky for permission to show and use its data. Constructive reviews by W. Heigl and an anonymous reviewer helped us improve the original manuscript.

Corresponding author: tary@ualberta.ca